Optics Letters

Phase-dependent interference between frequency doubled comb lines in a $\chi^{(2)}$ phase-matched aluminum nitride microring

Hojoong Jung,[1,†] Xiang Guo,[1,†] Na Zhu,[1] Scott B. Papp,[2] Scott A. Diddams,[2] and Hong X. Tang[1,*]

[1]Department of Electrical Engineering, Yale University, 15 Prospect Street, New Haven, Connecticut 06511, USA
[2]National Institute of Standards and Technology, 325 Broadway, Boulder, Colorado 80305, USA
*Corresponding author: hong.tang@yale.edu

Received 2 June 2016; revised 16 July 2016; accepted 18 July 2016; posted 20 July 2016 (Doc. ID 267509); published 4 August 2016

Nonlinear optical conversion with frequency combs is important for self-referencing and for generating shorter wavelength combs. Here we demonstrate efficient frequency comb doubling through the combination of second-harmonic generation (SHG) and sum-frequency generation (SFG) of an input comb with a high Q, phase-matched $\chi^{(2)}$ microring resonator. Phase coherence of the SHG and SFG nonlinear conversion processes is confirmed by sinusoidal phase-dependent interference between frequency doubled comb lines.

OCIS codes: (190.2620) Harmonic generation and mixing; (190.4223) Nonlinear wave mixing; (230.4320) Nonlinear optical devices; (230.5750) Resonators.

http://dx.doi.org/10.1364/OL.41.003747

Optical frequency combs are coherent broadband sources for spectroscopic sensing and precision metrology [1–4]. To expand these combs to shorter wavelength regions, harmonic generations from nonlinear materials are widely used. For example, Xe gas [5], beta-barium borate (BBO) [6,7], and periodically poled lithium niobate (PPLN) [8] crystals are used for nonlinear conversion of frequency comb in free space optics system. However, an on-chip frequency comb doubler is desirable for chip-integrated self-referencing of microcombs, as chip-based octave [9,10], or 2/3 octave microcombs [11], have recently been reported from silicon nitride (SiN) microrings. On-chip comb doubling has been reported from SiN [12] and aluminum nitride (AlN) [13] microrings simultaneously with microcomb generation. While SiN intrinsically has only relatively weak surface-induced Pockels effect, AlN has bulk $\chi^{(2)}$ nonlinearity (4.7 pm/V) [14], which easily enhances SHG.

In this Letter, we demonstrate on-chip efficient frequency doubling of an external mode locked fiber laser comb using a well-packaged phase-matched AlN microring resonator. In addition, a sinusoidal interference in the frequency doubled laser comb is observed by phase control of the input comb. The phase dependence of SHG was reported previously in a free space setup [15,16], using the pulse shaping technique. Our chip-integrated device shows more obvious sinusoidal curve with ∼0.9 visibility.

Figure 1(a) shows the experimental setup for efficient frequency doubling of the mode locked fiber laser comb. The mode locked fiber laser (Menlo systems) has a repetition rate (f_{rep}) of 250 MHz and bandwidth of more than 100 nm, as shown in Fig. 1(b). The laser passes a liquid-crystal-on-silicon (LCoS) programmable optical filter (denoted "waveshaper" by Finisar) that controls amplitude and phase with minimum bandwidth of ∼10 GHz. To probe SHG and SFG in the micro-resonator, we use the waveshaper to select comb lines (around 1550 nm) close to the resonances of an AlN microring. These selected comb lines are amplified to an average power of 100 mW with an erbium-doped fiber amplifier (EDFA); see Fig. 1(c). Each peak in Fig. 1(c) consists of ∼200 comb lines, depending on the waveshaper filter bandwidth setting. After passing a fiber polarization controller (FPC) and a wavelength division multiplexer (WDM), the amplified comb lines are coupled into the device under test (DUT) through a cleaved fiber with TM polarization. Only near-resonant comb lines can be enhanced in the microring resonator, in which second order nonlinear processes (including SFG and SHG) occur. The frequency doubled visible comb lines (near 775 nm) are coupled out of the device through the same fiber, and we measure them with an optical spectrum analyzer (OSA) after the WDM. Figure 1(d) shows the optical spectrum of the frequency doubled comb near 775 nm. Each peak here consists of ∼10 comb lines, which is determined by the number of input comb lines that fall within the IR microring resonance linewidth.

The schematics of the frequency conversion in the microring are shown in Fig. 2(a). The black lines represent the IR comb input and the red lines are the converted comb lines in the visible range. As shown in Fig. 1(c), the IR fiber comb is filtered using the waveshaper to keep comb lines near the resonances of the microring. Let us first consider only two comb bands. Each band has ∼200 comb lines with 250 MHz spacing, which covers 50 GHz of the spectrum around the IR fundamental TM (TM_{00}) modes [blue Gaussian curves in Fig. 2(a)]. For the AlN microring resonator,

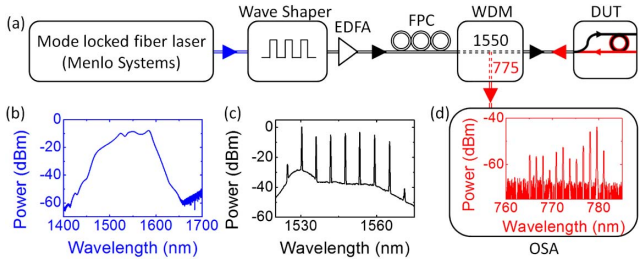

Fig. 1. (a) Experimental setup for efficient frequency comb doubling in an AlN mircoring. EDFA, erbium-doped fiber amplifier; FPC, fiber polarization controller; WDM, wavelength division multiplexer; DUT, device under test; OSA, optical spectrum analyzer. (b) The optical spectrum of a mode locked fiber laser comb with the 250 MHz repetition rate. (c) The spectrum of selected comb bands created with the waveshaper corresponding to the TM resonant modes of AlN microring. (d) The optical spectrum of doubled frequency comb lines through SHG and SFG.

the TM_{00} modes have free spectral range (FSR) of around 730 GHz and line width (Δf_{ring}) of 1 GHz. Therefore, in each resonance, there is an average of four comb lines. In the microring, only the near resonance comb lines [black solid lines in Fig. 2(a)] are enhanced and contribute to the frequency conversion process. With two IR comb bands input, each IR comb band generates a visible comb band at the doubled frequency through SHG and intraband SFG. An additional visible comb band comes from the interband SFG between the two IR comb bands. Because of the limited resolution of the OSA, each comb band is observed as a single peak in the OSA spectrum [Figs. 1(c) and 1(d)]. In fact, each band can be treated as a single line in an OSA, and this notation simplifies the discussion of the experimental results in the following.

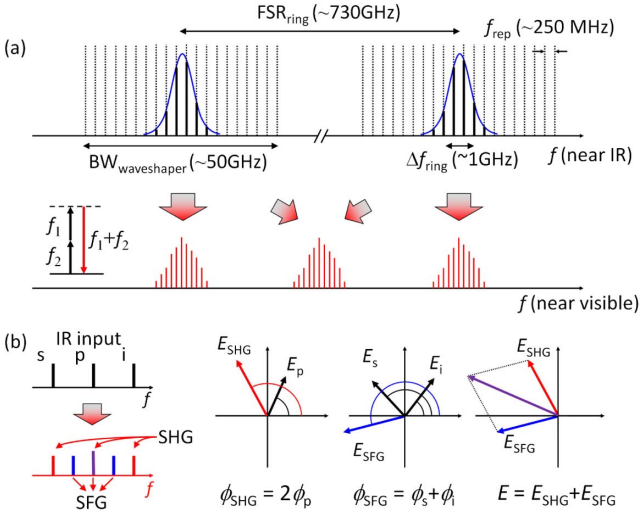

Fig. 2. (a) Schematic of frequency doubling for comb lines that are near resonance of the microring. Of the ~200 IR comb lines selected within the waveshaper bandwidth ($BW_{\text{waveshaper}}$), only approximately four comb lines fall in the ring resonance bandwidth and convert to the visible comb via SHG and SFG. In addition to the frequency doubled comb bands, another band comes from the SFG only between the two IR comb bands. (b) The principle of the phase-dependent interference between doubled frequencies. The amplitude of the final electric field (E) depends on the phase of E_{SHG} and E_{SFG}, or the input phase.

Figure 2(b) explains the interference between the generated SHG and SFG optical fields. In the left panel, three IR input lines generate three SHG lines (red) and three SFG lines (blue). The purple line at center arises from a combination of SHG and SFG. The electric fields of SHG and SFG are expressed as $E_{\text{SHG}} \exp(i\phi_{\text{SHG}}) \propto E_p^2 \exp(i(2\phi_p))$ and $E_{\text{SFG}} \exp(i\phi_{\text{SFG}}) \propto E_i E_s \exp(i(\phi_s + \phi_i))$, respectively, where E_p (E_s, E_i) is the central (left, right) IR line electric field amplitude and ϕ_p (ϕ_s, ϕ_i) is the corresponding electric field phase. After frequency conversion through SHG or SFG, the interference can be observed if the converted visible lines are involved in more than one conversion process. For example, the purple line comes from both SHG and SFG and the electric field is the summation of them: $E = E_{\text{SHG}} \exp(i\phi_{\text{SHG}}) + E_{\text{SFG}} \exp(i\phi_{\text{SFG}})$. As a result, the measured power has a term of $\cos(2\phi_p - \phi_s - \phi_i)$ that shows sinusoidal phase dependence. In this experiment, due to the minimum resolution bandwidth of the waveshaper and the 250 MHz spacing of the fiber comb, we cannot adjust the phase of each comb line individually, but rather the global phase of each comb section. Still, this limitation does not affect the interpretation of our experiments. The frequency of signal, pump, and idler comb band on resonance can be expressed by $f_s + mf_{\text{rep}}$ (m: 0 to i), $f_s + \text{FSR} + mf_{\text{rep}}$ (m: 0 to j), and $f_s + 2\text{FSR} + mf_{\text{rep}}$ (m: 0 to k), respectively, where f_s is the lowest frequency in the signal band on resonance and i, j, and k are the number of comb lines on each resonance, typically four. Then, the pump band is doubled and generates $2f_s + 2\text{FSR} + mf_{\text{rep}}$ (m: 0 to $2j$) through SHG and intraband SFG. The signal and idler IR bands also generate doubled frequencies at $2f_s + 2\text{FSR} + mf_{\text{rep}}$ (m: 0 to $i + k$) through interband SFG only. The frequencies of these lines are perfectly overlapped and give a phase-dependent interference. The mth electric field at doubled comb lines is expressed as $E_m = E_{\text{SHG}}^m \exp(i(2\phi_p)) + E_{\text{SFG}}^m \exp(i(\phi_s + \phi_i))$. Then the total power has the sinusoidal term of $\Sigma_{m=0}^{l} A_m \cos(2\phi_p - \phi_s - \phi_i)$, where l is the number of doubled comb lines that overlap and A_m is the SHG/SFG amplitude.

A microscope image of the device used in our experiments is shown in Fig. 3(a). The AlN microrings are 60 μm in diameter, and two waveguides are used for microring coupling to separately optimize IR and SHG/SFG wavelengths. The point-coupled waveguides above the microrings are for the IR light and the wrap-around waveguides below the microrings are for the SHG/SFG light. The wrap-around coupling gap and length are optimized for critical coupling, which is required for maximizing nonlinear conversion efficiency. Both waveguides are multiplexed to one waveguide for simple fiber-to-chip coupling. We simulate the phase-matching condition using the finite-element method (FEM) [Fig. 3(b)]. The IR fundamental mode and the visible third-order mode are matched to the same effective index when the waveguide width is ~1.12 μm, which corresponds to the microring waveguide width. Further fabrication details can be found in Ref. [17]. At the dual resonance conditions, the on-chip SHG conversion efficiency exceeds 1000%/W. Due to fiber-to-chip coupling loss, the packaged device, however, has lower conversion efficiency, 25%/W, from fiber to fiber.

The fiber and chip are permanently fixed using epoxy so an alignment-free frequency doubler can be conveniently sent between our laboratories in New Haven and Boulder, and potentially outside of a research lab [Fig. 3(c)]. Here the

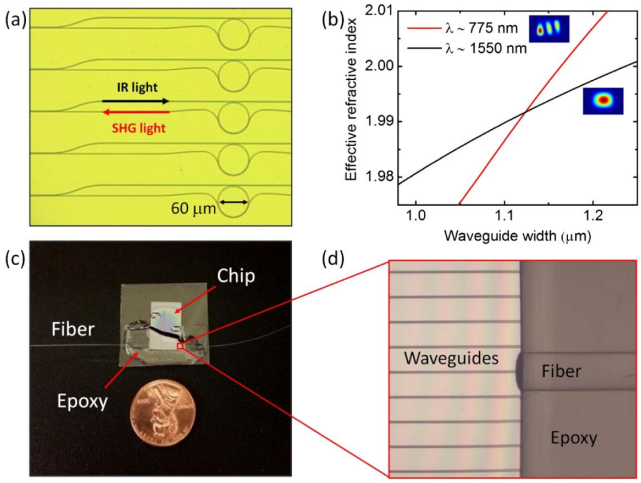

Fig. 3. (a) The top view of the fabricated device with microrings and two coupling waveguides for IR and visible lights. (b) The effective index simulation with different waveguide widths at 775 nm and 1550 nm wavelengths. (c) The packaged device with fixed fiber-to-chip alignment using an UV-curable epoxy. (d) The zoomed-in image of fiber to waveguide alignment with an average coupling efficiency of 30%.

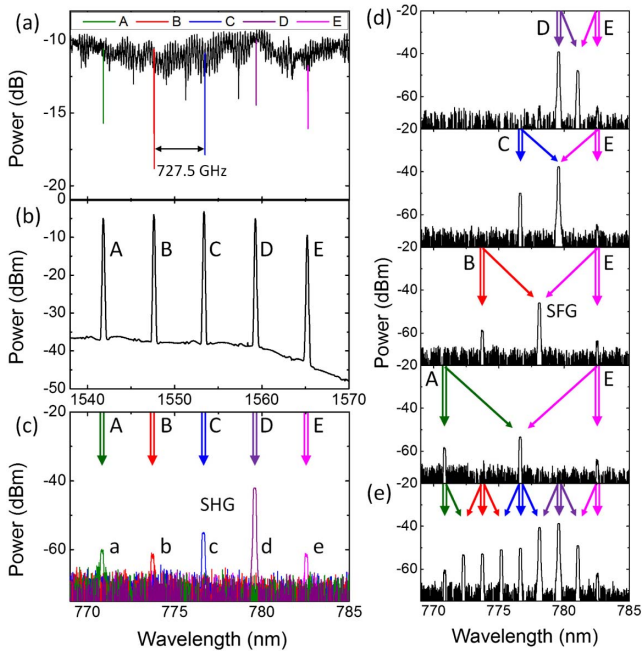

Fig. 4. (a) IR transmission spectrum of the AlN microring resonator with TM polarized input. (b) Selected comb bands corresponding to the five fundamental TM mode resonances. (c) SHG light from each comb band when tested one by one. (d) SFG lights from the combination of two inputs. (e) All possible SHG and SFG when all inputs ("A" to "E") are coupled to the microring.

UV light is used to cure the epoxy while maintaining the alignment of the fiber-to-chip interface. We achieve 10% fiber-to-fiber transmission with this relatively simple packaging scheme. Figure 3(d) shows a zoomed-in image of the waveguides and fiber under the cured epoxy. No drop in transmission is observed after the trip between different research labs, including commercial airline flights.

The experimental results of SHG and SFG are shown in Fig. 4. Here we show that the SHG and SFG processes can be characterized independently. Figure 4(a) is the IR transmission spectrum of the microring resonator device. A total of five fundamental TM modes are observed and their FSR is 727.5 GHz. Each resonance is named from "A" to "E" and denoted with different colors. As mentioned above, only comb lines near these five resonances are selected using the waveshaper. The spectrum of the IR pump bands selected by the waveshaper is shown in Fig. 4(b). Again, each peak actually consists of ~200 comb lines. First, SHG from each comb band is tested one by one, from "A" to "E" [Fig. 4(c)]. The generated SHG lights ("a"–"e") are strong enough to be measured with the OSA. The conversion efficiency of "D" to "d" is the strongest and "C" to "c" is the second, determined by the phase-matching condition. Next, we pick one more comb band to see SFG [Fig. 4(d)]. The comb band "E" is fixed and other inputs from "A" to "D" are tested one by one. All the combinations, "AE," "BE," "CE," and "DE" give interband SFG located between their respective frequency doubled band through SHG and intraband SFG, as expected. Figure 4(e) is the measured spectrum when all inputs ["A" to "E," as in Fig. 4(b)] are allowed for coupling to the microring. All combinations of SHG and SFG are possible and give 0.25 W^{-1} conversion efficiency. Each of these peaks in the visible range include ~10 comb lines with 250 MHz spacing as explained in Fig. 2(a).

Figure 5 shows phase-dependent interference of the visible light created via SHG and SFG. As explained above, we need to couple three IR comb bands ("C," "D," and "E") to the AlN microring to observe interference of the SHG and SFG. Specifically, we adjust the input phases of the IR comb bands one at a time from 0 to 2π using the waveshaper. When the phase of IR comb band "C" is adjusted, the visible power at frequency "d" is observed to vary, while all other peaks are stable; Fig. 5(a) shows the typical type of raw data we obtain. The observed power variation of "d" is extracted and plotted against the phase of band "C" [Fig. 5(b)]. It can be nicely fitted with a function of $P_d \propto \cos(\phi_C) + 1$. In a similar fashion, we change the phase of comb band "E" [see Figs. 5(c) and 5(d)] and also obtain similar power variation at frequency "d" due to SHG/SFG interference. This is because the comb bands "C" and "E" are located symmetrically around the center input comb band "D" and their roles are interchangeable in the SFG process. Finally, the phase of the comb band "D" is scanned, and doubled phase dependence is observed as shown in Figs. 5(e) and 5(f). The minimum and maximum powers can be reached when the phases are half π and π, respectively, which is determined by the function of $P_d \propto \cos(2\phi_D) + 1$. All three of these experiments varying the phases of comb bands "C," "D," and "E" result in observations that are well matched to the interference schematics of SHG and SFG shown in Fig. 2(b) and clearly indicate the relative contribution of SHG and SFG to the total harmonic power. The visibilities of the three cases [(b), (d), and (f)] are 0.886, 0.864, and 0.875, respectively. The nonzero minimum power is due to the amplitude mismatch between SHG and SFG electric fields with slightly different conversion efficiencies. This clear phase-dependent interference demonstration confirms the coherent

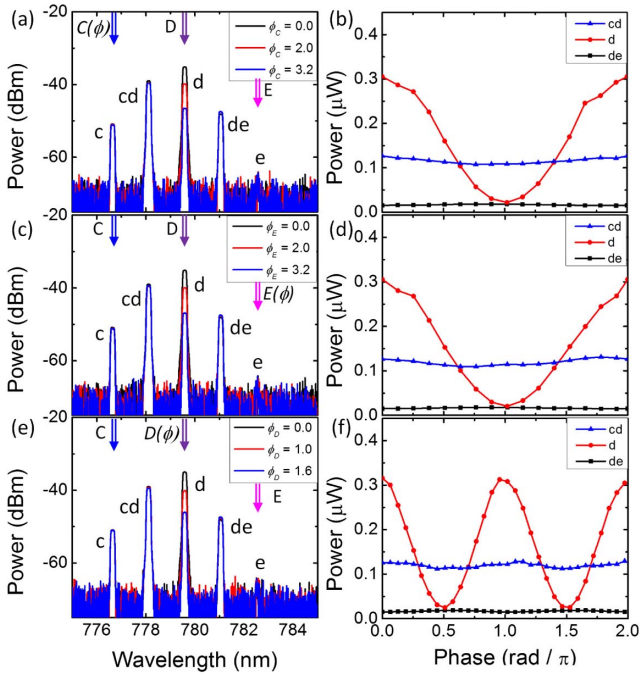

Fig. 5. Phase-dependent interference among the visible light generated via SHG and SFG. Spectra and power variations when the phase of input comb bands is adjusted [(a), (b)—"C,"(c), (d)—"E," and (e), (f)—"D"].

nature of frequency comb up-conversion in AlN microring resonators.

In conclusion, high efficiency SHG and SFG from a mode locked fiber frequency comb in AlN microring are demonstrated. Fiber-to-chip gluing techniques enable robust alignment-free performance after transport between labs and potentially outside the lab. The phase dependence during the frequency doubling is well matched with theory. Based on this clear sinusoidal curve, this device can be used as chip-based calibrator for line-by-line pulse shaping of a microcomb with a comparable f_{rep}.

Furthermore, chip-integrated $f-2f$ or $2f-3f$ self-referencing from octave or 2/3 octave microcombs are possible in AlN microrings. The high conversion efficiency enables on-chip direct doubling of a waveguide integrated Kerr comb without suffering from fiber-to-chip coupling loss. One concern is that the up-converted power might be too weak to measure due to weak microcomb lines powers. We estimate, however, with our current devices, a −30 dBm comb line can be up-converted to −80 dBm power, which is measurable with many commercial detectors. Once the on-chip detector is integrated, full-scale integration is foreseeable.

Funding. Defense Advanced Research Projects Agency (DARPA); National Science Foundation (NSF); National Institute of Standards and Technology (NIST).

Acknowledgment. Facilities used were supported by Yale Institute for Nanoscience and Quantum Engineering. We thank Michael Power and Dr. Michael Rooks for assistance in device fabrication.

†These authors contributed equally to this work.

REFERENCES

1. T. Udem, R. Holzwarth, and T. W. Hänsch, Nature **416**, 233 (2002).
2. S. T. Cundiff and J. Ye, Rev. Mod. Phys. **75**, 325 (2003).
3. D. J. Jones, S. A. Diddams, J. K. Ranka, A. Stentz, R. S. Windeler, J. L. Hall, and S. T. Cundiff, Science **288**, 635 (2000).
4. T. J. Kippenberg, R. Holzwarth, and S. A. Diddams, Science **332**, 555 (2011).
5. R. J. Jones, K. D. Moll, M. J. Thorpe, and J. Ye, Phys. Rev. Lett. **94**, 193201 (2005).
6. T. Ideguchi, A. Poisson, G. Guelachvili, T. W. Hänsch, and N. Picqué, Opt. Lett. **37**, 4847 (2012).
7. E. Peters, S. A. Diddams, P. Fendel, S. Reinhardt, T. W. Hänsch, and T. Udem, Opt. Express **17**, 9183 (2009).
8. S. Potvin and J. Genest, Opt. Express **21**, 30707 (2013).
9. Y. Okawachi, K. Saha, J. S. Levy, Y. H. Wen, M. Lipson, and A. L. Gaeta, Opt. Lett. **36**, 3398 (2011).
10. Q. Li, T. C. Briles, D. Westly, J. Stone, R. Ilic, S. Diddams, S. Papp, and K. Srinivasan, *Frontiers in Optics*, OSA Technical Digest (online) (Optical Society of America, 2015), paper FW6C.5.
11. V. Brasch, M. Geiselmann, T. Herr, G. Lihachev, M. H. P. Pfeiffer, M. L. Gorodetsky, and T. J. Kippenberg, Science **351**, 357 (2016).
12. S. Miller, K. Luke, Y. Okawachi, J. Cardenas, A. L. Gaeta, and M. Lipson, Opt. Express **22**, 26517 (2014).
13. H. Jung, R. Stoll, X. Guo, D. Fischer, and H. X. Tang, Optica **1**, 396 (2014).
14. W. H. P. Pernice, C. Xiong, C. Schuck, and H. X. Tang, Appl. Phys. Lett. **100**, 223501 (2012).
15. V. V. Lozovoy, I. Pastirk, and M. Dantus, Opt. Lett. **29**, 775 (2004).
16. Z. Zheng and A. M. Weiner, Opt. Lett. **25**, 984 (2000).
17. X. Guo, C.-L. Zou, C. Schuck, H. Jung, and H. X. Tang, "Parametric down-converted photon-pair source on a silicon chip platform," arXiv:1603.03726v1.